CALPHAD: Computer Coupling of Phase Diagrams and Thermochemistry 35 (2011) 355–366

Contents lists available at ScienceDirect

CALPHAD: Computer Coupling of Phase Diagrams and Thermochemistry

journal homepage: www.elsevier.com/locate/calphad

An improved thermodynamic modeling of the Fe–Cr system down to zero kelvin coupled with key experiments

Wei Xiong [a,*], Peter Hedström [a], Malin Selleby [a], Joakim Odqvist [a], Mattias Thuvander [b], Qing Chen [c]

[a] Department of Materials Science and Engineering, KTH (Royal Institute of Technology), SE-100 44 Stockholm, Sweden

[b] Department of Applied Physics, Chalmers University of Technology, SE-412 96 Göteborg, Sweden

[c] Thermo-Calc Software AB, Norra Stationsgatan 93, SE-113 64 Stockholm, Sweden

ARTICLE INFO

Article history:
Received 12 March 2011
Received in revised form
2 May 2011
Accepted 11 May 2011

Keywords:
Phase separation
Stainless steels
Atom probe
Ab initio calculations
Heat capacity
Magnetic

ABSTRACT

A thermodynamic modeling of the Fe–Cr system down to 0 K is performed on the basis of our recent comprehensive review of this binary system [W. Xiong, M. Selleby, Q. Chen, J. Odqvist, Y. Du, Evaluation of phase equilibria and thermochemical properties in the Fe–Cr system, Crit. Rev. Solid State Mater. Sci. 35 (2010) 125–152]. The model predicts a sign change for the magnetic ordering energy of mixing rather than the enthalpy of mixing in the bcc phase at 0 K. Designed key experiments are performed not only to check the validity of the present modeling but also to assist in understanding the mechanism for spinodal decomposition of the Fe–Cr alloy. Heat capacities and Curie temperatures of several Fe-rich alloys are determined between 320 and 1093 K by employing differential scanning calorimetry. The measured heat capacities are found to be in remarkable agreement with the prediction based on the present modeling. Microstructural patterns and frequency distribution diagrams of Cr are studied in alloys containing 26.65, 31.95, and 37.76 at.% Cr by using atom probe tomography. The observed phase separation results correspond well with our model-predicted boundary for the spinodal decomposition. Interestingly, a horn on the Cr-rich spinodal boundary is predicted below 200 K for the first time. This work demonstrates a way to bridge the ab initio calculations and CALPHAD approach.

1. Introduction

The Fe–Cr system is the basis for many materials of practical importance, e.g. stainless steels, structural reactor materials, and interconnect materials of solid oxide fuel cells. Numerous studies have been devoted to study its properties. A well-known feature of the Fe–Cr system is the miscibility gap of the bcc (body centered cubic) phase at low temperatures. Inside the miscibility gap, alloys tend to separate or decompose into a Cr-rich bcc phase (α') and an Fe-rich bcc phase (α) [1]. Due to this phase separation, Fe–Cr alloys have been found to exhibit an increased hardness and decreased ductility after aging, which is historically known as the "475 °C embrittlement" [2]. For duplex stainless steels, the decomposition and consequent embrittlement of the ferritic phase effectively sets an upper limit for the service temperature. To investigate the mechanisms controlling the decomposition in duplex stainless steels, a reliable thermodynamic description of the Fe–Cr is vital. However, as discussed in our review on this system [3], there is no such description yet.

So far, there are at least ten different thermodynamic descriptions of the Fe–Cr system available in the literature [4–14]. Among these, the commonly accepted one is due to Andersson and Sundman [9], but this description, as pointed out recently by Xiong et al. [3], needs to be improved in many aspects, among which a better representation of experimental Curie temperatures is especially important. Without a good reproduction of the measured data on the magnetic phase diagram, the accuracy of the magnetic contribution to the Gibbs energy cannot be guaranteed [15].

It should also be noticed that recently the amount of research on Fe–Cr alloys increases rapidly [3]. One of the reasons is the sign change of the enthalpy of mixing (H_{mix}) at 0 K for the ferromagnetic bcc phase from negative to positive on the Fe-rich side predicted by the ab initio calculations [16]. Since it is impossible to perform such an experiment at extremely low temperature to study the phase equilibria in the Fe–Cr alloys, the ab initio calculated H_{mix} with a simplified magnetic treatment has influenced not only some other type of ab initio based computational simulations (e.g. ab initio Monte Carlo) but also some subjective judgments on the experimental observations on the Fe–Cr alloys (see Ref. [3] and its comments made on some publications refer to the bcc miscibility gap). Although in our previous review [3] and some recent ab initio calculations [17,18], the accuracy of the ab

* Corresponding author. Tel.: +46 8 790 8313; fax: +46 8 100411.
E-mail addresses: wxiong@yahoo.com, wei@mse.kth.se (W. Xiong).

0364-5916/$ – see front matter © 2011 Elsevier Ltd. All rights reserved.
doi:10.1016/j.calphad.2011.05.002

Table 1
The experimental Curie temperatures of the alloys determined in this work.

No.	x_{Cr}, at.%	T_C/K
1	1.159	1051
2	3.365	1054
3	6.767	1046
4	9.921	1030
5	13.050	1007

Table 2
Chemical composition (wt.%) for materials used in the APT study[a].

No.	Cr	C	Si	Mn	P	S	Ni	N
SFC6	25.28	0.002	0.09	0.09	0.004	0.006	0.03	0.009
SFC7	30.42	0.004	0.06	0.111	0.006	0.008	0.02	0.006
SFC8	36.1	0.005	0.27	0.09	0.005	0.005	0.02	0.008

[a] In this work, SFC6, SFC7 and SFC8 are considered with 26.65, 31.95, and 37.76 at.% Cr, respectively.

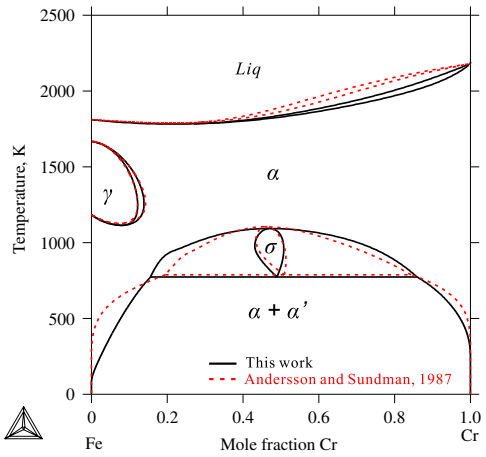

Fig. 1. (Color online) Comparison of the calculated phase diagram between the present thermodynamic description and the one by Andersson and Sundman [9].

initio predicted enthalpy of mixing for the bcc phase has been questioned obviously, it is of great interest to make an attempt to quantitatively check the validity of the ab initio predictions [16]. To this end, a thermodynamic modeling down to 0 K is necessary. In the present work, a revised lattice stability for pure Fe down to 0 K reported by Chen and Sundman [19] is adopted so that one could extend the thermodynamic modeling down to 0 K at the Fe-rich side, and thus make some quantitative comparison with the ab initio results.

In view of the above, the purpose of the present work was to perform a thermodynamic modeling of the Fe–Cr system down to 0 K and obtain some reasonable predictions of the thermodynamic properties at low temperatures. The heat capacity of some Fe-rich alloys was determined in order to validate the present thermodynamic modeling. For the sake of studying spinodal decomposition, the microstructure in the Fe–Cr binary alloys was studied by employing the atom probe tomography (APT), and could be explained by using the present thermodynamic modeling.

2. Experimental details

2.1. DSC measurements

Five alloys were designed and prepared for heat capacity determination using Differential Scanning Calorimetry (DSC). The alloys were prepared in the Central South University, PR China

Table 3
Summary of the optimized thermodynamic parameters of the Fe–Cr system[a].

Liquid: model (Cr, Fe)	
${}^0L^{Liq}_{Cr,Fe} = -5.983 \cdot T$	${}^1L^{Liq}_{Cr,Fe} = -384.41$
α: model (Cr, Fe)	
${}^0L^{bcc}_{Cr,Fe} = 24\,212.06 - 15.507 \cdot T$	${}^1L^{bcc}_{Cr,Fe} = 1664.69 + 0.286 \cdot T$
${}^2L^{bcc}_{Cr,Fe} = -13\,250.88 + 8.252 \cdot T$	${}^0\beta^{bcc}_{Cr,Fe} = -0.45$
${}^0T^{bcc}_C = 865.5$	${}^1T^{bcc}_C = -567.2$
γ: model (Cr, Fe)	
${}^0L^{fcc}_{Cr,Fe} = 28\,871.89 - 22.318 \cdot T$	${}^1L^{fcc}_{Cr,Fe} = 32\,711.42 - 18.180 \cdot T$
σ: model $(Cr, Fe)_{10}(Cr, Fe)_{20}$	
${}^oG^{\sigma}_{Cr:Cr} - 30 \cdot {}^oG^{bcc}_{Cr} = 150\,000$	
${}^oG^{\sigma}_{Cr:Fe} - 10 \cdot {}^oG^{bcc}_{Cr} - 20 \cdot {}^oG^{bcc}_{Fe} = -13\,807.14 - 10.715 \cdot T$	
${}^oG^{\sigma}_{Fe:Cr} - 10 \cdot {}^oG^{bcc}_{Fe} - 20 \cdot {}^oG^{bcc}_{Cr} = 313\,807.14 + 10.715 \cdot T$	
${}^oG^{\sigma}_{Fe:Fe} - 30 \cdot {}^oG^{bcc}_{Fe} = 150\,000$	
${}^0L^{\sigma}_{Cr,Fe:Cr} = {}^0L^{\sigma}_{Cr,Fe:Fe} = 7722.64 - 139.766 \cdot T$	
${}^0L^{\sigma}_{Cr:Cr,Fe} = {}^0L^{\sigma}_{Fe:Cr,Fe} = 89\,908.52 - 156.894 \cdot T$	

[a] The parameters can be used for calculation in the newest version of Thermo-Calc S with the modified magnetic model proposed by Chen and Sundman [19]. The unit of energy is in J mol atoms^{-1}, temperature (T) in Kelvin. The Gibbs energy for pure Fe is from the work by Chen and Sundman [19], while the one for pure Cr is taken from the SGTE compilation [22].

withan arc-melter (Bühler Mini arc melting system MAM-1, Edmund Bühler GmbH, Germany) on a water-cooled copper plate under argon atmosphere. The raw materials were elemental Fe and Cr (both with a purity of 99.99 wt.%, Alpha Products, Johnson Matthey Company, USA). Each alloy was re-melted four times to ensure homogeneity. The weight loss during arc melting was kept below 1 wt.%. Inductively coupled plasma-atomic emission spectrometry (ICP-AES, ADVANTAGE-1000, TJA) was used to analyze the Cr content in the prepared alloys, see Table 1.

Measurements of the heat capacity were conducted in the DSC apparatus (NETZSCH STA 449C, Netzsch, Germany) by using the ASTM E1269 method. The derivation of the heat capacities of the samples is as follows:

$$C_P^{Sample} = \frac{m_{Sample}}{m_{Standard}} \cdot \frac{S_{Sample} - S_{Baseline}}{S_{Standard} - S_{Baseline}} \cdot C_P^{Standard} \quad (1)$$

where m, S, and C_P denotes the mass, signal and heat capacity of the standard or the sample, respectively. Synthetic sapphire was used as the standard in the present measurement according to the ASTM-norm. The DSC measurements were performed with a heating rate of 10 K/min in dynamic pure argon atmosphere (purity of 99.999%) between 320 and 1093 K with the flow rate of 20 ml/min.

2.2. APT measurements

Three ingots for APT were provided by Sandvik AB in Sweden. The ingots (c.a. 600 g for each) were produced by vacuum arc melting. Samples for APT were homogenized at 1100 °C for 2 h under argon and subsequently quenched in brine. Table 2 shows the chemical compositions for the three alloys denoted SFC6, SFC7 and SFC8 with 26.65, 31.95 and 37.76 at.% Cr, respectively.

Aging of the samples was performed at 500 °C for different periods of time. Samples for APT were selected from both as-homogenized conditions as well as phase separated conditions as indicated by micro-hardness measurements. The samples were first cut to 20 × 0.3 × 0.3 mm^3 and subsequently sharp needle-like samples for APT were prepared using the standard two-stage

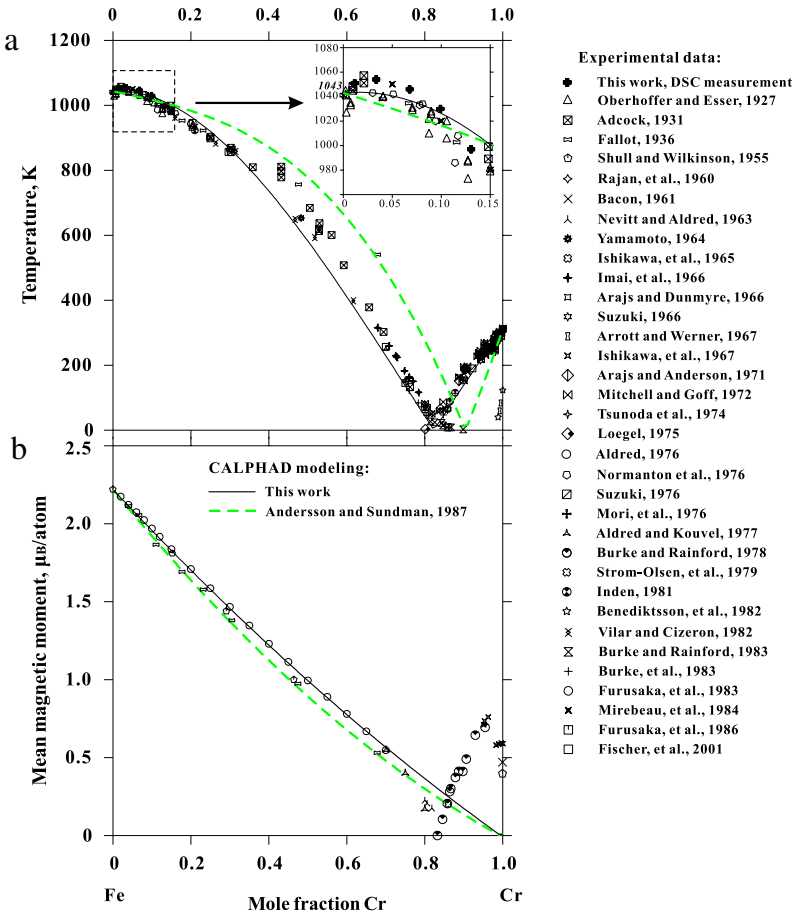

Fig. 2. (Color online) The magnetic phase diagram of the Fe–Cr system. Comparison of the (a) Curie temperature and (b) mean magnetic moment curves between experiments and thermodynamic descriptions from this work and the one by Andersson and Sundman [9]. Experimental data are taken from the review by Xiong et al. [3].

electro-polishing method. The analyses were performed using a local electrode atom probe (LEAP 3000X HR^{TM}, Imago Scientific Instruments, USA) equipped with a reflectron for improved mass resolution. The ion detection efficiency is about 37%, as specified by the supplier. The experiments were made in voltage pulse mode (20% pulse fraction, 200 kHz, evaporation rate 1.5%) with a specimen temperature of 55 K.

3. Thermodynamic modeling

Before setting different thermodynamic models for the different phases in the Fe–Cr system, a comprehensive literature survey on the Fe–Cr system was performed and reported separately as a review [3]. Therefore, detailed information on the reported experiments can be achieved from our previous work [3].

3.1. Lattice stability of pure elements

At present, a new type of description for the lattice stability of Fe assessed by Chen and Sundman [19] was adopted and therefore allows a good description of thermodynamic properties of pure Fe down to 0 K. In the same work of Chen and Sundman [19], the magnetic model proposed by Inden [20] and Hillert and Jarl [21] has been reformulated for a relatively more accurate description of the magnetic effect in the bcc phase of pure Fe. Hence, the modified magnetic model has also been taken into account in this work. It should be mentioned that this new magnetic formulation is implemented in Thermo-Calc software version S due to this work.

According to Chen and Sundman [19], the Gibbs energy of the bcc phase for pure Fe can be expressed as:

$$G = E_0 + \frac{3}{2}R\cdot\Theta_E + 3RT\ln\left[1-\exp\left(-\frac{\Theta_E}{T}\right)\right] - \frac{a}{2}T^2 - \frac{b}{20}T^5 - \int_0^T\left[\int_0^T\frac{C_P^{mag}}{T}dT\right]dT \quad (2)$$

in which E_0 is the total energy of the ferromagnetic bcc structure at 0 K. The second term corresponds to the energy of zero-point lattice vibration, and the third term consists the electronic excitations and low-order anharmonic corrections. Parameter a can be related to the electron density of states at the Fermi level, while parameter b reflects the high-order anharmonic lattice vibrations. Θ_E is the Einstein temperature, which is 309 K for pure Fe. For further information of the revised lattice stability of pure Fe, please see the work by Chen and Sundman [19].

As discussed by Xiong et al. [3], there are still lots of problems for the CALPHAD method to make an accurate description of pure Cr, e.g. in the thermodynamic evaluation on pure elements by SGTE (Scientific Group Thermodata Europe) [22], the melting point of pure Cr has been overestimated, and a hypothetic small Bohr magnetic moment has been assigned to Cr due to its weak magnetic contribution to the heat capacity in the vicinity of the Néel temperature. Since the above problem needs more specific individual investigations including model development (such as

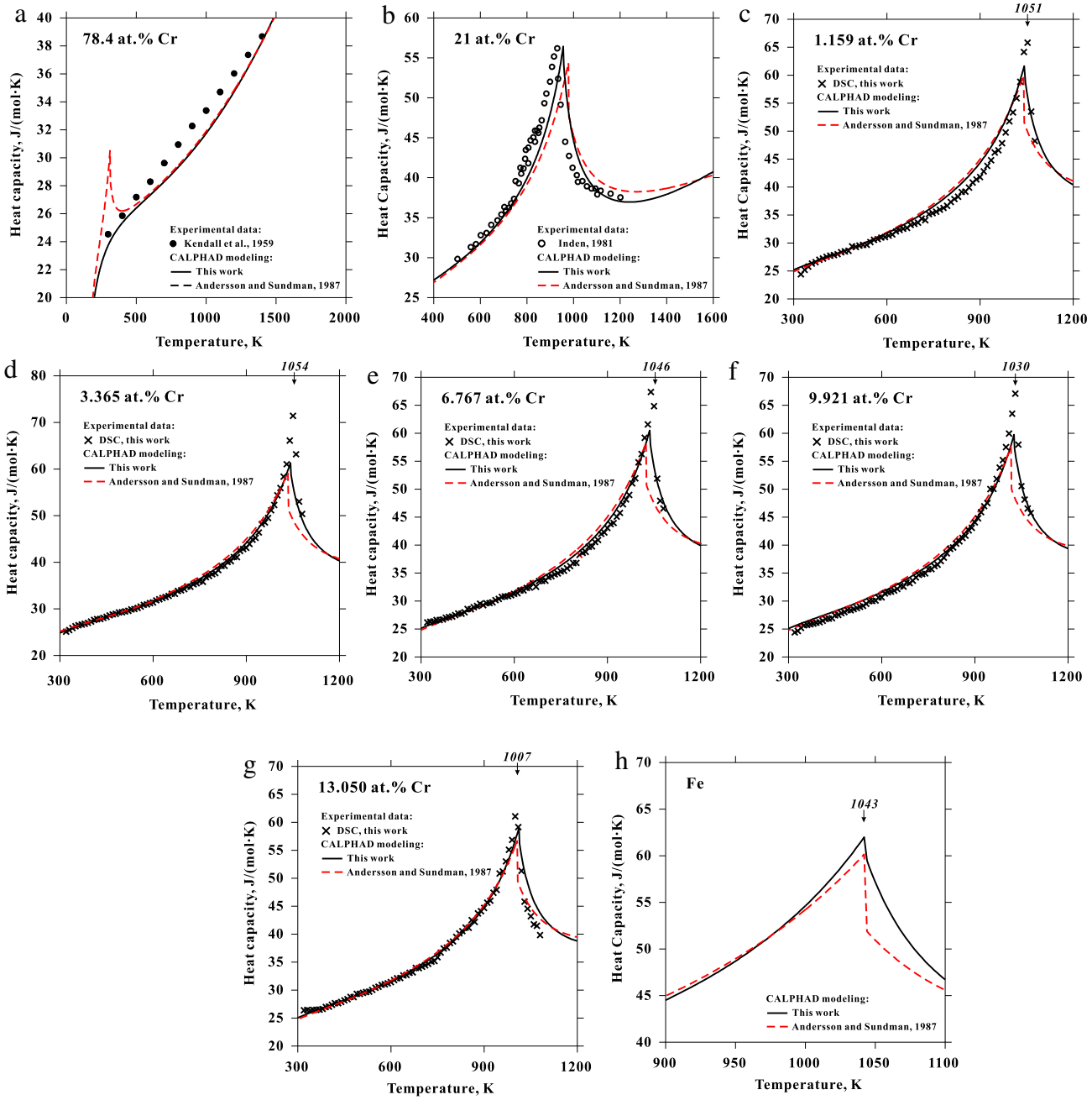

Fig. 3. (Color online) Comparisons of the heat capacity of the alloys with Cr content of (a) 21 at.%; (b) 78.4 at.%; (c) 1.159 at.%; (d) 3.365 at.%; (e) 6.767 at.%; (f) 9.921 at.% (g) 13.050 at.%; and (h) pure Fe, among the thermodynamic prediction, the experimental data and the reported experiments by Inden [20] and Kendall et al. [26].

the composition dependence of the magnetic contribution), this work has not attempted to revise the thermodynamic description of pure Cr. Moreover, it is believed that this will not bring any noticeable impact on the present topic since the major interest of spinodal decomposition in stainless steels concerns alloys with less than 30 at.% Cr.

It is worth to mention that the new magnetic model by Chen and Sundman [19] has been extrapolated into the binary system, which means that the same type of changes for the magnetic model has been applied to pure Cr. However, this will not have any apparent influence on the magnetic contribution to the Gibbs energy of pure Cr, since such a contribution from magnetic ordering in the case of pure Cr is intrinsically very small [23].

3.2. Models of solution and intermetallic phases

The substitutional solution model has been adopted for the description of theliquid, α (body centered cubic structure) and γ (face centered cubic structure) phases. The thermodynamic model for the σ phase (topologically close packed structure), which is the only intermetallic phase in the Fe–Cr system, has been adopted as proposed by Joubert [24]. Joubert suggested a simplified two-sublattice model, $(Cr, Fe)_{10}(Cr, Fe)_{20}$, based on the composition range of the σ phase in different systems for construction of multicomponent thermodynamic databases. The molar Gibbs energy of the σ phase is given accordingly by the

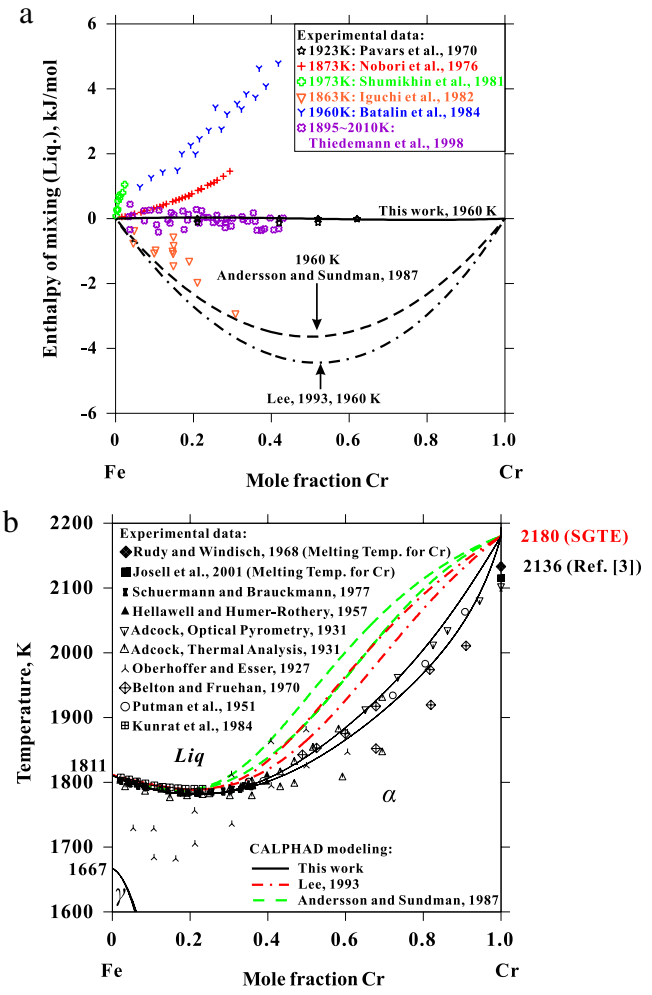

Fig. 4. (Color online) Phase equilibria and properties in the liquid phase region. (a) Comparison of H_{mix} of the liquid phase between experiments and calculations; (b) Comparison of the phase equilibria with the liquid phase involved. The melting temperature of pure Cr suggested by Xiong et al. [3] is 2136 K.

following expression:

$$\begin{aligned} G_m^{\sigma} = {} & y'_{Cr}y''_{Fe}\cdot {}^{o}G^{\sigma}_{Cr:Fe} + y'_{Cr}y''_{Cr}\cdot {}^{o}G^{\sigma}_{Cr:Cr} \\ & + y'_{Fe}y''_{Cr}\cdot {}^{o}G^{\sigma}_{Fe:Cr} + y'_{Fe}y''_{Fe}\cdot {}^{o}G^{\sigma}_{Fe:Fe} \\ & + 10RT[(y'_{Cr}\ln y'_{Cr} + y'_{Fe}\ln y'_{Fe}) + 2(y''_{Cr}\ln y''_{Cr} + y''_{Fe}\ln y''_{Fe})] \\ & + (y'_{Cr}y''_{Cr}y''_{Fe}\cdot L_{Cr:Cr,Fe} \\ & + y'_{Fe}y''_{Cr}y''_{Fe}\cdot L_{Fe:Cr,Fe} + y'_{Cr}y'_{Fe}y''_{Fe}\cdot L_{Cr,Fe:Fe} \\ & + y'_{Cr}y'_{Fe}y''_{Fe}\cdot L_{Cr,Fe:Fe} + y'_{Cr}y'_{Fe}y''_{Cr}y''_{Fe}\cdot L_{Cr,Fe:Cr,Fe}) \end{aligned} \quad (3)$$

where y'_{Cr}, y''_{Cr}, y'_{Fe} and y''_{Fe} represent the site fraction of Cr/Fe in the first/second sublattice. L is the interaction parameter between different species in the same sublattice, and can be expanded in a Redlich–Kister polynomial [25]. It is worth to note that an alternative three-sublattice model, $(Cr, Fe)_{10}(Cr, Fe)_4(Cr, Fe)_{16}$, mentioned in the same work by Joubert [24] could also be considered, but the difference between these two models is only significant in extrapolating to multicomponent systems with considerable homogeneity ranges of σ.

3.3. Thermodynamic optimization

The parameters were evaluated by the optimization module PARROT in Thermo-Calc version S. In terms of the previous literature review [3], different weights have been assigned to the reliable experimental data during the thermodynamic modeling. The comparison between these experimental data and the present calculated results will be discussed further in the next section. It should be emphasized that the experimental data obtained in this work has not been used in the optimization but instead used to validate the present thermodynamic modeling. A set of self-consistent thermodynamic parameters from the present modeling is given in Table 3.

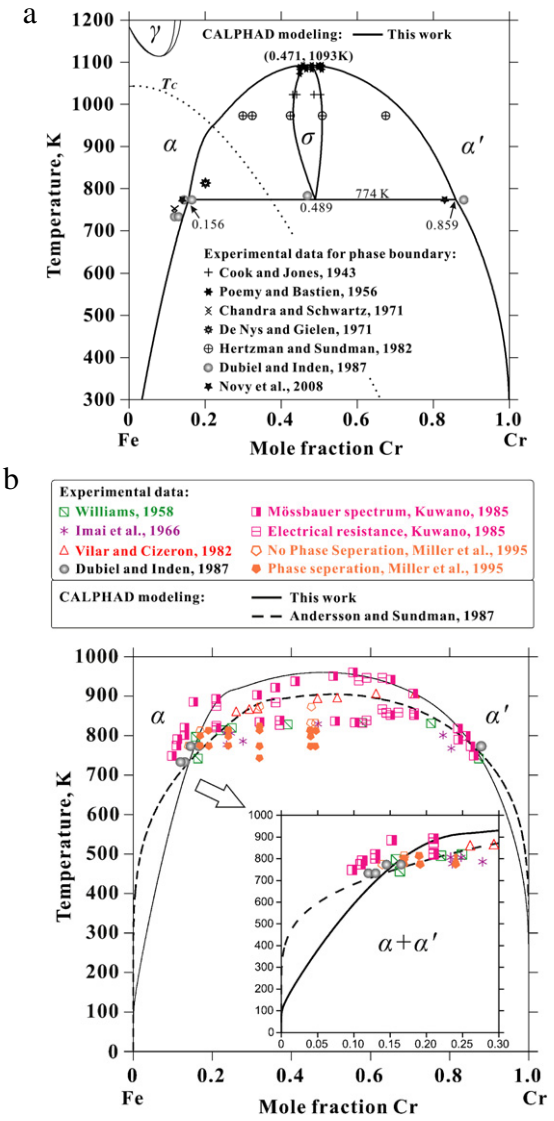

Fig. 5. Low temperature phase equilibria in the Fe–Cr system: (a) Stable phase equilibria for the σ and bcc phases (dotted line shows the calculated Curie temperature for homogeneous α solution in this work). The values of compositions and temperatures for some critical phase transition points are denoted; (b) (Color online) Comparison of the metastable miscibility gap and the phase boundary on the Fe-rich side between modeling and experiments.

4. Results and discussion

According to the present thermodynamic modeling, the Fe–Cr phase diagram has been updated as shown in Fig. 1. It should be noted that most of the phase boundaries have been revised according to thecomprehensive evaluation by Xiong et al. [3], except for the γ-loop, which shows no significant difference with

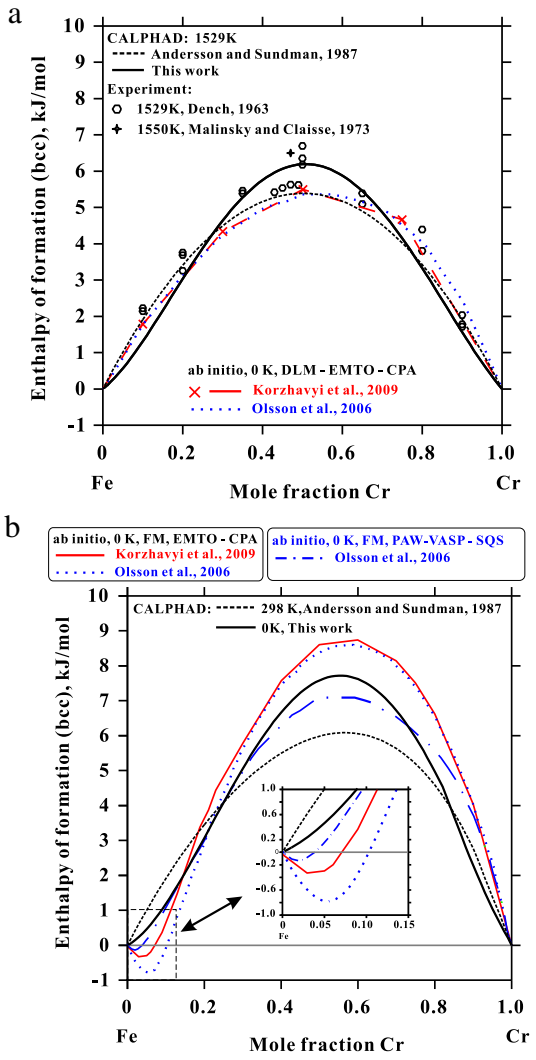

Fig. 6. (Color online) Thermodynamic properties of the bcc phase in the Fe–Cr system (a) Comparison of H_{mix} for the α phase at 1529 K among experiments [34,35], ab initio DLM calculations [18,36] and thermodynamic modeling in this work and the one by Andersson and Sundman [9]; (b) Comparison of H_{mix} for the α phase at 0 K between the ab initio results [18,36] and thermodynamic modeling in this work and in Andersson and Sundman [9].

the previous modeling [9]. The features of the phase diagram and thermodynamic properties will be discussed in this section based on our experimental results from calorimetry and APT.

4.1. Curie temperature and heat capacity

The Curie temperature curve with a maximum at around 3 at.% Cr estimated by Xiong et al. [3] has been confirmed by the DSC measurements in this work. As shown in Fig. 2(a), the Curie temperature at 3.36 at.% Cr, according to the present experiment, is 11 K higher than for pure Fe, 1043 K. However, it is found that the description of a small maximum of the Curie temperature will not only require a large number of parameters in the form of Redlich–Kister polynomials [25] but also cause trouble in fitting the experimental Curie temperatures in the higher Cr content region.

As shown in Fig. 3, good agreement can be easily found between the calculated heat capacities and the experimental results from this work and previous reports [20,26]. Generally, the present modeling shows a better agreement with the experimental data than theassessment by Andersson and Sundman [9]. Moreover, in the vicinity of the Curie temperature, the present modeling shows a smooth curve for the heat capacity in the magnetic short range order region (i.e. above the Curie temperature). In contrast, there is an abrupt change in the calculated curve in the previous thermodynamic modeling [9]. This comes from the thermodynamic description of pure Fe, and is more apparent in Fig. 3(h). Thus, it indicates the advantage of adopting the revised lattice stability of Fe [19].

4.2. High temperature phase equilibria and H_{mix} of liquid

The enthalpy of mixing of the liquid phase is rather scattered compared with the H_{mix} of the solid bcc phase which will be described in the next section. As shown in Fig. 4(a), the previous assessments by Andersson and Sundman [9] and Lee [14] agree with the experimental data by Iguchi et al. [27]. Contrarily, the current thermodynamic modeling predicts that liquid Fe–Cr alloys exhibit almost ideal behavior, which is in good agreement with experimental data by Pavars et al. [28] and Thiedemann et al. [29].

Regarding the equilibria of the liquid phase, the recommended experimental data by Adcock [30] and Putman et al. [31] in the earlier review by Xiong et al. [3] have been considered as the most reliable input in this work for assessing the liquid phase as shown in Fig. 4(b).

It should be kept in mind that the melting temperature of pure Cr was suggested to be 2136 K [3] instead of 2180 K as adopted currently by SGTE [22]. Since the lattice stability of Cr was not reassessed in the present work, the improvement of the thermodynamic description above 90 at.% Cr is limited. Despite of this, it is found that the large deviation from the experimental liquidus as in the previous assessments [9,14] (see Fig. 4(b)) can easily generate the negative value of H_{mix} for the liquid phase as shown in Fig. 4(a).

4.3. Low temperature phase equilibria and H_{mix} of α

In Fig. 5, the stable phase diagram at low temperatures with the σ and bcc phases was calculated according to the present optimization. Good agreement can be found between the present modeling and experimental data by Dubiel and Inden [32] who determined the phase diagram from extra-long term annealed samples. It should be emphasized that the phase boundary between $\alpha + \sigma$ and α as determined by Hertzman and Sundman [4] should not be considered as reliable data, since the authors found that the samples with two phases (α and σ) were still far from the equilibrium state due to the low number of nuclei of σ [4]. This is also the reason why these data have not been considered in the thermodynamic description by Hertzman and Sundman [4]. According to the present modeling, the decomposition temperature of the σ phase is 774 K which is in the evaluated range between 773 and 783 K by Xiong et al. [3].

A comparison of the metastable bcc miscibility gap between modeling and experiments is shown in Fig. 5(b). The calculated miscibility gap is in good agreement with the accepted experimental data by Kuwano [3,33]. The consolute temperature is 960 K, i.e. 56 K higher than the one by Andersson and Sundman [9], in good agreement with the evaluation by Xiong et al. [3] (~970 K).

A comparison of H_{mix} of the α phase at around 1529 K between thermodynamic modeling [9] and experiments [34,35] is given in Fig. 6(a). The calculations in the present work and the previous one [9] can both well reproduce the experimental data which is rather symmetric. However, as shown in Fig. 6(b), the predicted H_{mix} ofthe α phase at 0 and 298 K shows a rather asymmetrical profile. Furthermore, the ab initio calculations in the ferromagnetic

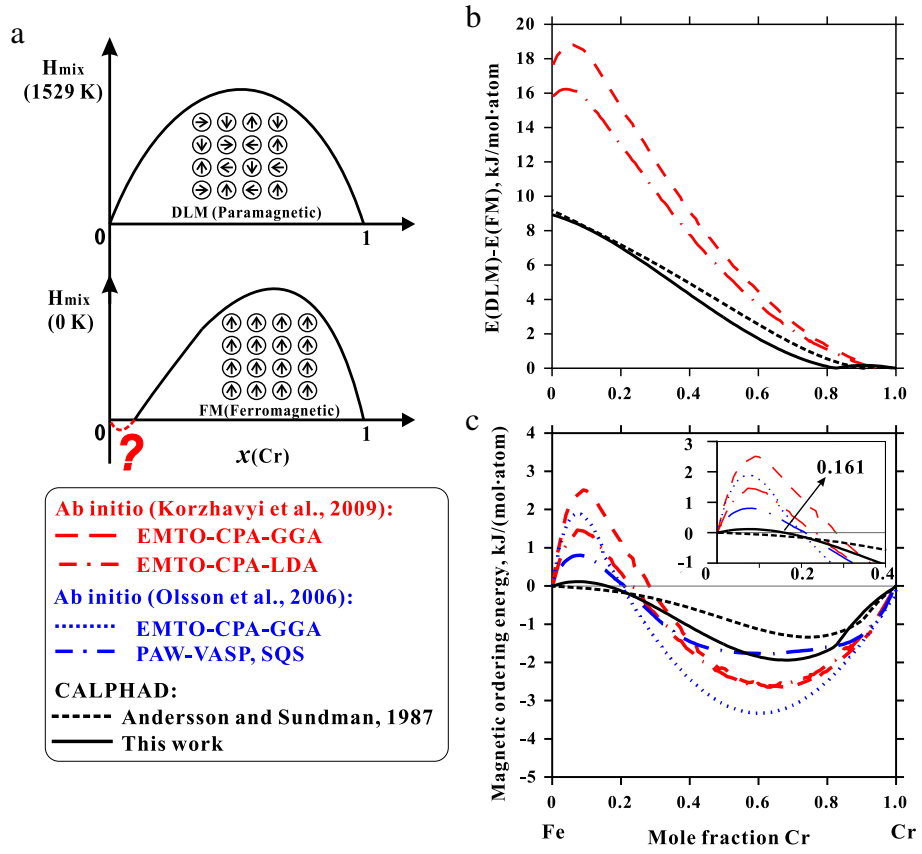

Fig. 7. (a) A sketch showing the feature of enthalpy of mixing according to experiments [34,35] and ab initio calculations [18,36]; (b) Comparison of MOE between ab initio calculations [18,36] and thermodynamic modeling; (c) Comparison of MOEM between ab initio calculations [18,36] and thermodynamic modeling. (For interpretation of the references to color in this figure legend, the reader is referred to the web version of this article.)

states using different models conducted by different groups [18,36] show a negative value of H_{mix} on the Fe-rich side, which indicates a certain solubility of Cr in (α-Fe) at 0 K. In the present thermodynamic modeling, it is found that any attempt to introduce such solubility of Cr in (α-Fe) at 0 K will both prevent a reasonable representation of the experimental H_{mix} for the α phase at 1529 K, and result in a much higher consolute temperature than given by experiments [33]. In view of this, one should be aware of that the ab initio prediction at 0 K deserves some further studies due to the unsophisticated treatment on the Cr-rich side. The treatment using the ferromagnetic state (but not antiferromagnetism or spin density wave [37,38]) on the Cr-rich side in the ab initio calculations is certainly a rough simplification, and will introduce unpredictable uncertainty for the results on the Fe-rich side.

In order to understand the difficulties of fitting H_{mix} at both temperatures, 0 and 1529 K, by thermodynamic modeling, an illustration of the magnetic contribution to the Gibbs energy is shown in Fig. 7. Two different physical quantities discussed in the previous work [3] are recalculated according to the present thermodynamic description. One is the difference between the heat of mixing of the paramagnetic (or disordered local moment (DLM)) and ferromagnetic (FM) states, E (DLM) − E (FM), which represents the absolute value of the magnetic ordering energy (MOE), and the other one is the so-called magnetic ordering energy of mixing (MOEM) [3], which shows alloying effect on the magnetic ordering energy. As can be seen, for pure Fe, the ab initio calculations show nearly a double value for MOE compared to the thermodynamic modeling. In addition, there is a strong tendency of maximum in the contribution from magnetism. Nevertheless, in the present thermodynamic modeling, a small positive value can be generated for MOEM (see Fig. 7(c)) which can be understood as a contribution from the magnetic short range ordering effects [3]. Still, it is far from the large positive values needed to accommodate the ab initio calculations. However, the model-predicted sign change of MOEM in this work probably can be interpreted as a contribution to the short range order (SRO) inversion effects which was firstly found in an early calculation by Hennion [39] by using tight-binding generalized perturbation method at 0 K, and later experimentally reported at 703 K with 11 at.% Cr by Mirebeau et al. [40,41].

So far, there are no experimental data in phase equilibria indicating that Cr is soluble in (α-Fe) at 0 K [3]. Moreover, it is noteworthy that in some other atomistic simulations (e.g. embedded-atom method [42]), the calculated consolute temperature will be incredibly high (~2700 K) [42] if Cr is assumed to have some solubility in (α-Fe) at 0 K.

After the intensive discussion on the modeling of the α phase, it is necessary to make a short note on the recent efforts of the ab initio studies of the σ phase [11,12,28,43–49]. By using the Mössbauer technique and ab initio calculations, the entropy difference between the σ and α phase has been determined in the work of Dubiel et al. [46], which were consistent with the modeling by Houserová et al. [11]. One shall also bear in mind that due to the ferromagnetism of the σ phase below about 50 K [50,51] the magnetic contribution to the total energy in the atomistic calculations needs to be taken into account [45,47,48].

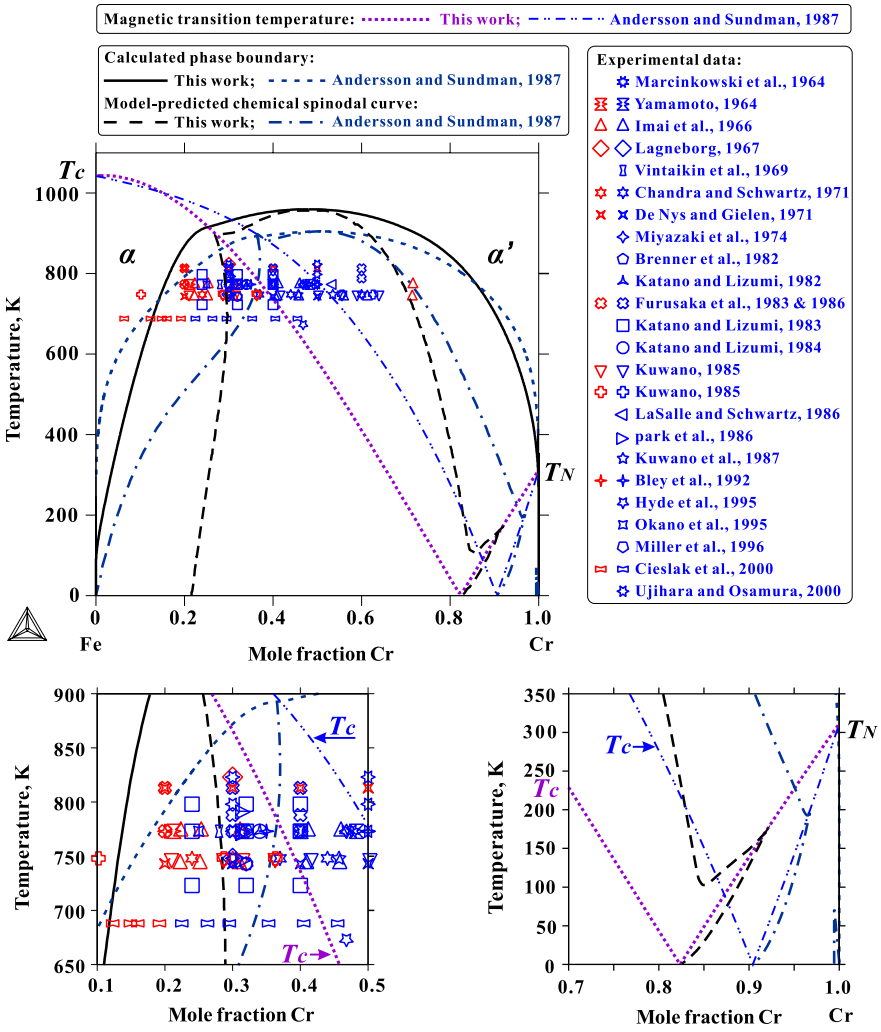

Fig. 8. Comparison of the chemical spinodal line between model prediction and experimental data. Experimental data can be found in the compilation by Xiong et al. [3]. The blue symbols represent the alloys in the spinodal dominating regime, the red ones are in the nucleation and growth dominating regime. The magnetic transition temperature curve according to the present work is presented as dotted line in purple, while the one from the previous work [9] is given as chained line in blue. (For interpretation of the references to color in this figure legend, the reader is referred to the web version of this article.)

Because of the foregoing discussion on magnetic properties, atomistic simulations of the Fe–Cr system with high accuracy become a formidable task.

4.4. Phase separation and microstructure evolution

4.4.1. Model-predicted spinodal curve

The chemical spinodal based on the present thermodynamic modeling and the previous modeling by Andersson and Sundman [9] is plotted in Fig. 8 compared with available experimental data collected in the work of Xiong et al. [3]. Due to the small difference in atomic size between Fe and Cr, it is commonly believed that the difference between the coherent and chemical spinodal is small. Compared with Andersson and Sundman [9], the spinodal predicted from the new modeling is closer to the Fe-rich side above 650 K and almost vertical to the composition axis over the whole temperature range (see Fig. 8).

It should be emphasized that, the model-predicted spinodal region on the Fe-rich side at 0 K shown in Fig. 8 is at 21.7 at.% Cr, which is different with a simple extrapolation from the previous modeling [9]. The present calculated results are not contradicting to the prediction from ab initio calculations [17] that the pair interactions show a sign change on the Fe-rich side from ordering to clustering. One could envisage that MOEM shown in Fig. 7(c) is the cause of such an SRO effect which deserves more detailed ab initio calculations by incorporating magnetic effects explicitly [17].

Interestingly, even though the phase boundary on the Cr-rich side is rather smooth, a horn on the spinodal line due to the antiferromagnetic effects can be found (see the right bottom zoom-in in Fig. 8). Instead of having a well-developed horn, Andersson and Sundman's description [9], which is not meant for low temperature equilibrium of course, gives an isolated small cusp-like spinodal curve at above 99 at.% Cr.

4.4.2. Comparison between modeling and experiments

It is expected that there is no sharp transition from nucleation and growth to spinodal decomposition [52,53]. Rather, there is a transient region showing both features. This could also be one of the reasons why both spinodal decomposition and nucleation and growth can be observed in the vicinity of 30 at.% Cr by the different experiments in Fig. 8. Furthermore, some of the differences in

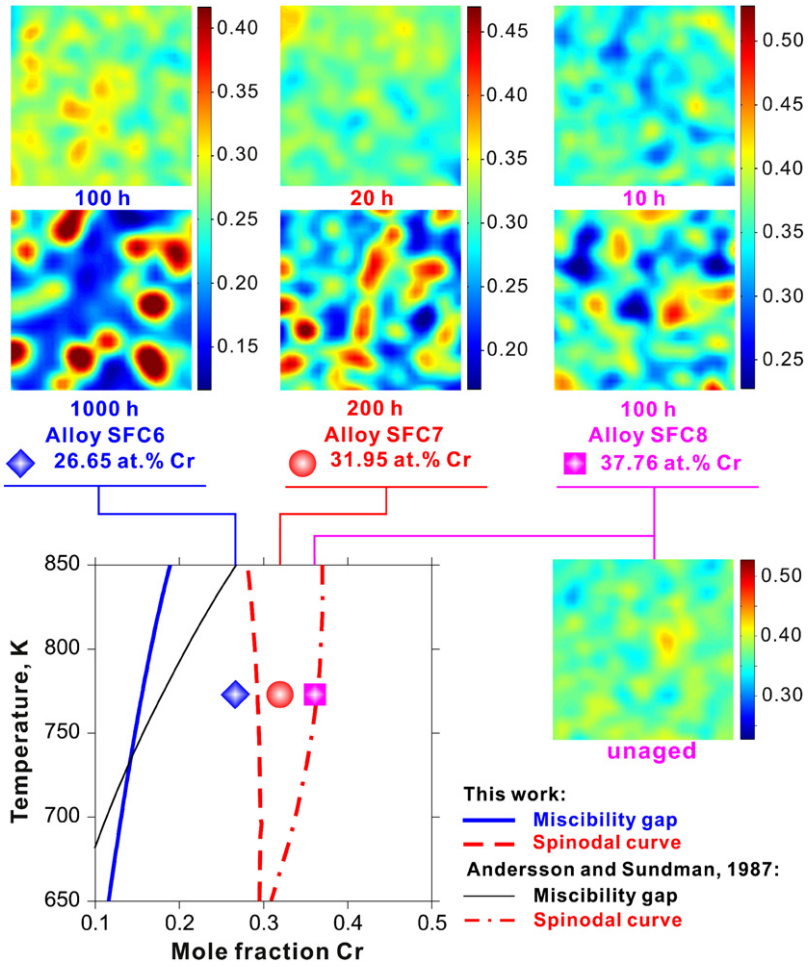

Fig. 9. 2D concentration maps of Cr in the aged alloys with 26.65, 31.95 and 37.76 at.% Cr measured by APT. The size of the concentration contour patterns is 30 × 30 nm^2. The chemical compositions of the alloys are indicated in the phase diagram at the bottom. (For interpretation of the references to color in this figure legend, the reader is referred to the web version of this article.)

the literature may stem from the difficulty in identifying the different phases in a decomposed structure as well as experimental difficulties to define sub-nano nuclei.

The evolution of the microstructure during phase separation from the homogeneous state of the unaged alloys to the clearly phase separated state was studied from the 3D-APT (three dimensional atom probe tomography) data using 3D iso-concentration surface, 3D atom maps of Cr, and 2D (two dimensional) concentration maps of Cr. The 2D concentration maps (see Fig. 9) were constructed using a cube size (voxel size) of 1 nm^3 and the upper and lower limit of the concentration scale was set to 15 at.% from the average concentration in the material. It should be mentioned that the appearance of the 3D iso-concentration surfaces are sensitive to the concentration threshold used and hence the presentation in Fig. 9 is judged to be a fairly unbiased qualitative description of the microstructure.

Frequency distributions of Cr constructed using 25 ions per group are presented in Fig. 10, together with the corresponding random (binomial) distribution. As the detection efficiency is 37% and the lattice parameter of the bcc structure is 0.287 nm, the size of each group is 0.80 nm^3. In the unaged condition, the measured distribution is close to the random distribution as shown in Fig. 10(c). After heat treatment at 773 K, the measured distributions start to deviate from the random distribution and becomes wider, which is indicative of a phase separation [54] as shown in Fig. 10.

According to the model-predicted spinodal curve in this work, alloy SFC6 is just outside the chemical spinodal, and thus may be located in a transient region. It is noticed that the frequency distribution of alloy SFC6 is quite asymmetric (see Fig. 10(a)) and could be considered as an overlap of two peaks. The weak peak on the Cr-rich side is in the vicinity of 60 at.% Cr, which is inside the miscibility gap. As shown in Fig. 9, the 2D concentration maps of Cr of alloy SFC6 (26.65 at.% Cr) aged for 1000 h clearly shows that the isolated particles dominated the microstructure. This indicates that the non-classical nucleation is the governing mechanism for the phase separation of alloy SFC6. This agrees with the results presented by Miller [55] where an alloy with 25.3 at.% Cr aged at 773 K had both isolated islands and a 3D interconnected structure.

Regarding alloy SFC7 with 31.95 at.% Cr, the frequency distribution diagram in Fig. 10(b) for the sample aged for 200 h becomes asymmetric and much wider than the one aged for 20 h. This coincides with the 2D concentration maps of Cr plotted in Fig. 9, in which both a 3D interconnected structure and areas with isolated islands can be observed after 200 h aging. As shown in the phase diagram (see Fig. 9), alloy SFC7 is just inside the chemical spinodal, and thus also in a transient region between spinodal decomposition and nucleation and growth regimes.

In contrast to alloys SFC6 and SFC7, it is found that the frequency distribution diagram for alloy SFC8 in Fig. 10(c) was widening faster when the aging time increased. Only after 100 h of aging,

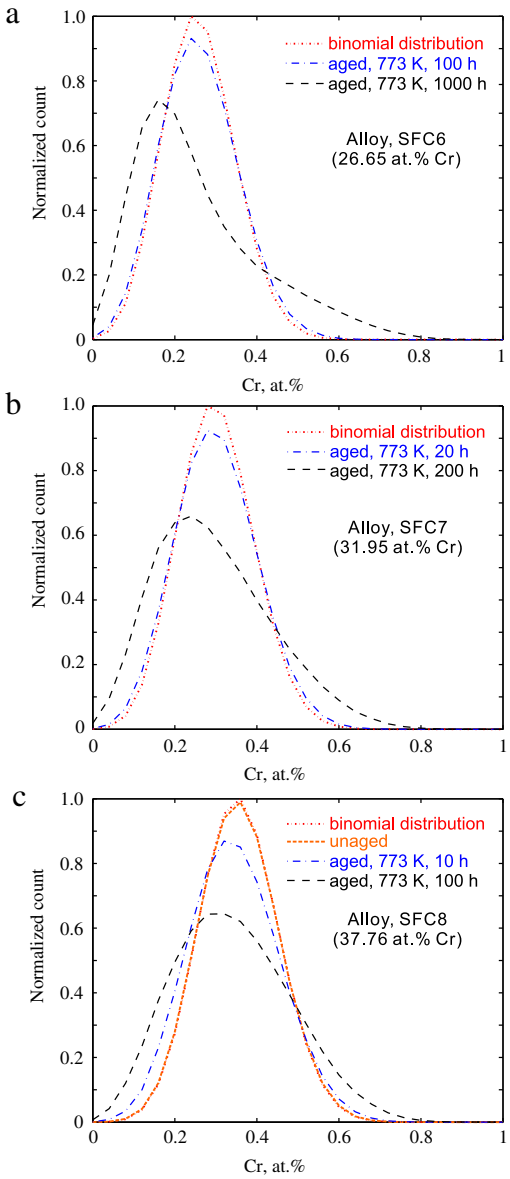

Fig. 10. Frequency distribution diagrams of Cr, constructed using 25 ions per group for different alloys with (a) 26.65, (b) 31.95, and (c) 37.76 at.% Cr determined by APT. (For interpretation of the references to color in this figure legend, the reader is referred to the web version of this article.)

the peak of the frequency diagram shows a comparable full width at half maximum to the one of alloy SFC7 aged for 200 h, and the center of its peak has less deviation from the one of the binomial distribution.

As can be observed in the 2D concentration maps of Cr in Fig. 9, the interconnected structure dominates the microstructure of alloy SFC8. Furthermore, the determined 3D atom maps of the Cr distribution with the size of 30 × 15 × 8 nm^3 (see Fig. 11) show clearly that the amount of the interconnected structure increases with the Cr content. This can be well explained by the present thermodynamic modeling, since alloy SFC8 is clearly inside the chemical spinodal. The above observations also support the evaluation by Xiong et al. [3] that a transition region can be found within the composition limit from 24–36.3 at.% Cr and the temperature range between 700 and 830 K.

In view of the above, the APT results are in good agreement with the model-predicted spinodal curve in this work. Despite of the transient region in the vicinity of the chemical spinodal curve, it is expected that the present thermodynamic modeling will provide more accurate driving forces for spinodal decomposition, which are essential for simulating the microstructural evolution using the phase field technique.

5. Conclusions

(1) A thermodynamic modeling by using the revised lattice stability of pure Fe down to 0 K was performed for the Fe–Cr system. Significant improvements are visible by comparison of the phase diagram and thermodynamic properties between this work and previous assessments [9,14]. The present work shows a promising way to improve the current thermodynamic databases of alloy systems.

(2) The successful implementation of the revised lattice stability of pure Fe could act as a template for some other thermodynamic descriptions concerning low temperature thermodynamics. Therefore, it is worth to revise the lattice stability of pure Cr further using an analogous way as for pure Fe by Chen and Sundman [19]. Improvements of the magnetic model are also needed because of the problems found in the magnetic phase diagrams of Fe–Cr and Fe–Ni in our previous work [15].

(3) In this work, heat capacities of Fe-rich alloys were determined by DSC measurements. The present modeling generally shows better agreement with the experimental heat capacities, compared with the previous modeling. A small maximum on the Curie temperature curve at about 3 at.% was confirmed experimentally.

(4) The present thermodynamic description rules out the possibility to introduce any solubility of Cr in (α-Fe) at 0 K predicted by the ab initio calculations which are computed at ferromagnetic states of the Fe–Cr alloys. However, a positive value of MOEM on the Fe-rich side can still be predicted in the present modeling.

(5) The model-predicted spinodal curve is different from the one by Andersson and Sundman [9]. The chemical spinodal limit on the Fe-rich side starts from 21.7 at.% Cr at 0 K. A horn on the Cr-rich spinodal curve was found and deserves further study.

(6) The 3D-APT data clearly indicate a transition from nucleation and growth to spinodal decomposition in the prepared alloys. Alloys with 26.65 and 31.95 at.% Cr are inside the region with a transition regime between nucleation and growth and spinodal decomposition, while the one with 37.76 at.% Cr close to the edge of the transition region and mainly shows the behavior like spinodal decomposition. The experimental observations are well explained by the model-predicted spinodal curve, which also validates the present thermodynamic description.

Acknowledgments

This work was performed within the VINN Excellence Center Hero-m, financed by VINNOVA, the Swedish Government Agency of Innovation Systems, Swedish Industry and KTH. The operation of the DSC measurement by Dr. T. Matsushita (KTH) and sample preparation assisted by Prof. Yong Du in the Central South University, China are greatly appreciated. JO and MT acknowledge the financial support from the Swedish Research Council (Grant No. 621-2009-5289). Mr. Saeed Bagsheikhi is acknowledged for help with heat treatments and hardness measurements. Dr. Magnus Boström (Sandvik Materials Technology) is acknowledged for providing the experimental alloys for APT. Authors are grateful to Dr. Pavel A. Korzhavyi, Profs. John Ågren, Andrei V. Ruban and Prof. Emeritus Mats Hillert (KTH) for stimulating discussions.

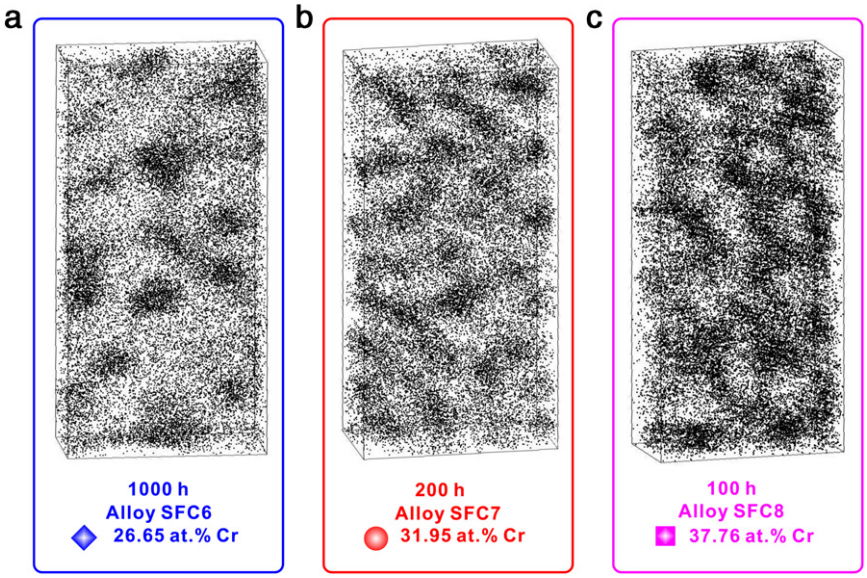

Fig. 11. (Color online) Atom maps of the Cr distribution for alloys with (a) 26.65, (b) 31.95, and (c) 37.76 at.% Cr determined by APT. The size of the box for analysis is $30 \times 15 \times 8$ nm^3.

Appendix. Supplementary data

Supplementary material related to this article can be found online at doi:10.1016/j.calphad.2011.05.002.

References

[1] R.M. Fisher, E.J. Dulis, K.G. Carroll, Identification of the precipitate accompanying 885F embrittlement in chromium steels, Trans. Am. Inst. Min. Metall. Pet. Eng. 197 (1953) 690–695.
[2] F.M. Becket, On allotropy of stainless steels, Trans. Am. Inst. Min. Metall. Pet. Eng. 131 (1938) 15–36.
[3] W. Xiong, M. Selleby, Q. Chen, J. Odqvist, Y. Du, Evaluation of phase equilibria and thermochemical properties in the Fe–Cr system, Crit. Rev. Solid State Mater. Sci. 35 (2010) 125–152.
[4] S. Hertzman, B. Sundman, A thermodynamic analysis of the Fe–Cr system, CALPHAD 6 (1982) 67–80.
[5] J.O. Andersson, A thermodynamic evaluation of the Fe–Cr–C system, TRITA-MAC-0207, KTH, 1982.
[6] L. Kaufman, Proceedings of the forth calphad meeting, CALPHAD 1 (1977) 7–89.
[7] Y.Y. Chuang, J.C. Lin, Y.A. Chang, A thermodynamic description and phase relationships of the Fe–Cr system: part I the BCC phase and the sigma phase, CALPHAD 11 (1987) 57–72.
[8] J.C. Lin, Y.Y. Chuang, K.C. Hsieh, Y.A. Chang, A thermodynamic description and phase relationships of the Fe–Cr system: part II the liquid phase and the FCC phase, CALPHAD 11 (1987) 73–81.
[9] J.O. Andersson, B. Sundman, Thermodynamic properties of the Cr–Fe system, CALPHAD 11 (1987) 83–92.
[10] X. Liu, S. Hao, An analysis on interaction parameters of binary solid solutions, CALPHAD 17 (1993) 67–78.
[11] J. Houserová, M. Friák, M. Šob, J. Vřešťál, Ab initio calcualtions of lattice stability of sigma-phase and phase diagram in the Cr–Fe system, Comput. Mater. Sci. 25 (2002) 562–569.
[12] J. Vřešťál, J. Houserová, M. Šob, Energetics and phase diagrams of Fe–Cr and Co–Cr systems from first principles, J. Min. Metall. Sect. B 38 (2002) 205–211.
[13] J. Tomiska, The system Fe–Ni–Cr: revision of the thermodynamic description, J. Alloys Compd. 379 (2004) 176–187.
[14] B.-J. Lee, Revision of thermodynamic descriptions of the Fe–Cr and Fe–Ni liquid phases, CALPHAD 17 (1993) 251–268.
[15] W. Xiong, H. Zhang, L. Vitos, M. Selleby, Magnetic phase diagram of the Fe–Ni system, Acta Mater. 59 (2011) 521–530.
[16] P. Olsson, I.A. Abrikosov, L. Vitos, J. Wallenius, Ab initio formation energies of Fe–Cr alloys, J. Nucl. Mater. 321 (2003) 84–90.
[17] A.V. Ruban, P.A. Korzhavyi, B. Johansson, First-principles theory of magnetically driven anomalous ordering in BCC Fe–Cr alloys, Phys. Rev. B: Condens. Matter Mater. Phys. 77 (2008) 094436.
[18] P.A. Korzhavyi, A.V. Ruban, J. Odqvist, J.O. Nilsson, B. Johansson, Electronic structure and effective chemical and magnetic exchange interactions in BCC Fe–Cr alloys, Phys. Rev. B: Condens. Matter Mater. Phys. 79 (2009) 054202.
[19] Q. Chen, B. Sundman, Modeling of thermodynamic properties for BCC, FCC, liquid, and amorphous iron, J. Phase Equilib. 22 (2001) 631–644.
[20] G. Inden, The role of magnetism in the calculation of phase diagrams, Physica B+C 103 (1981) 82–100.
[21] M. Hillert, M. Jarl, A model for alloying in ferromagnetic metals, CALPHAD 2 (1978) 227–238.
[22] A.T. Dinsdale, SGTE data for pure elements, CALPHAD 15 (1991) 317–425.
[23] J.O. Andersson, Thermodynamic properties of chromium, Int. J. Thermophys. 6 (1985) 411–419.
[24] J.M. Joubert, Crystal chemistry and Calphad modeling of the σ phase, Prog. Mater. Sci. 53 (2008) 528–583.
[25] O. Redlich, A.T. Kister, Algebraic representation of thermodynamic properties and the classification of solutions, Ind. Eng. Chem. 40 (1948) 345–348.
[26] W.B. Kendall, R.L. Orr, R. Hultgren, AFOSR-TN-59-524, 1959, pp. 1–14.
[27] Y. Iguchi, S. Nobori, K. Saito, T. Fuwa, Calorimetric study of heats of mixing of liquid iron alloys Fe–Cr, Fe–Mo, Fe–W, Fe–V, Fe–Nb, Fe–Ta, Tetsu to Hagane 68 (1982) 633–640.
[28] I.A. Pavars, B.A. Baum, P.V. Gel'd, Thermophysical and thermodynamic properties of liquid alloys of iron and chromium, High Temp. 8 (1970) 67–71.
[29] U. Thiedemann, M. Roesner-Kuhn, D.M. Matson, G. Kuppermann, K. Drewes, M.C. Flemings, M.G. Frohberg, Mixing enthalpy measurements in the liquid ternary system iron–nickel–chromium and its binaries, Steel Res. 69 (1998) 3–7.
[30] F. Adcock, Alloys of iron research part X—the chromium–iron constitutional diagram, J. Iron. Steel Inst. 124 (1931) 99–149.
[31] J.W. Putman, R.D. Potter, N.J. Grant, The ternary system chromium–molybdenum–iron, Trans. Am. Soc. Met. 43 (1951) 824–852.
[32] S.M. Dubiel, G. Inden, On the miscibility gap in the Fe–Cr system: a moessbauer study on long term annealed alloys, Z. Metkd. 78 (1987) 544–549.
[33] H. Kuwano, Moessbauer effect study on the miscibility gap of the iron–chromium binary system, Trans. Japan Inst. Met. 26 (1985) 473–481.
[34] W.A. Dench, Adiabatic high-temperature calorimeter for measurement of heats of alloying, Trans. Faraday Soc. 59 (1963) 1279–1292.
[35] I. Malinsky, F. Claisse, A high-temperature calorimeter, J. Chem. Thermodyn. 5 (1973) 615–622.
[36] P. Olsson, I.A. Abrikosov, J. Wallenius, Electronic origin of the anomalous stability of Fe-rich BCC Fe–Cr alloys, Phys. Rev. B: Condens. Matter Mater. Phys. 73 (2006) 104416.
[37] E. Fawcett, Spin-density-wave antiferromagnetism in chromium, Rev. Modern Phys. 60 (1988) 209–283.
[38] P.G. Evans, E.D. Isaacs, G. Aeppli, Z. Cai, B. Lai, X-ray microdiffraction images of antiferromagnetic domain evolution in chromium, Science 295 (2002) 1042–1045.
[39] M. Hennion, Chemical SRO effects in ferromagnetic Fe alloys in relation to electronic band structure, J. Phys. F: Met. Phys. 13 (1983) 2351–2358.
[40] I. Mirebeau, M. Hennion, G. Parette, First measurement of short-range-order inversion as a function of concentration in a transition alloy, Phys. Rev. Lett. 53 (1984) 687–690.
[41] I. Mirebeau, G. Parette, Neutron study of the short range order inversion in $Fe_{1-x}Cr_x$, Phys. Rev. B: Condens. Matter Mater. Phys. 82 (2010) 104203.
[42] G. Bonny, R.C. Pasianot, L. Malerba, A. Caro, P. Olsson, M.Y. Lavrentiev, Numerical prediction of thermodynamic properties of iron–chromium alloys using semi-empirical cohesive models: the state of the art, J. Nucl. Mater. 385 (2009) 268–277.

[43] K. Chvátalová, J. Houserová, M. Šobb, J. Vrešťál, First-principles calculations of energetics of sigma phase formation and thermodynamic modelling in Fe–Ni–Cr system, J. Alloys Compd. 378 (2004) 71–74.
[44] M. Šob, A. Kroupa, J. Pavlů, J. Vřešťál, Application of ab initio electronic structure calculations in construction of phase diagrams of metallic systems with complex phases, Diffus. Defect Data Part B 150 (2009) 1–28.
[45] J. Pavlů, J. Vřešťál, M. Šob, Ab initio study of formation energy and magnetism of sigma phase in Cr–Fe and Cr–Co systems, Intermetallics 18 (2010) 212–220.
[46] S.M. Dubiel, J. Cieslak, W. Sturhahn, M. Sternik, P. Piekarz, S. Stankov, K. Parlinski, Vibrational properties of alpha- and sigma-phase Fe–Cr alloy, Phys. Rev. Lett. 104 (2010) 155503.
[47] E.A. Kabliman, A.A. Mirzoev, A.L. Udovskii, First-principles simulation of an ordered sigma phase of the Fe–Cr system in the ferromagnetic state, Phys. Met. Metall. 108 (2009) 435–440.
[48] E. Kabliman, P. Blaha, K. Schwarz, A.V. Ruban, B. Johansson, Ab initio-based mean-field theory of the site occupation in the Fe–Cr sigma-phase, Phys. Rev. B: Condens. Matter Mater. Phys. 83 (2011) 092201.
[49] Z.K. Liu, First-principles calculations and CALPHAD modeling of thermodynamics, J. Phase Equilib. Diffus. 30 (2009) 517–534.
[50] Y. Sumitomo, T. Moriya, H. Ino, F.E. Fujita, The Mossbauer effect of Fe–V and Fe–Cr sigma phase, J. Phys. Soc. Japan 35 (1973) 461–468.
[51] D.A. Read, E.H. Thomas, J.B. Forsythe, Evidence of itinerant electron ferromagnetism in sigma phase alloys, J. Phys. Chem. Solids 29 (1968) 1569–1572.
[52] K. Binder, P. Fratzl, Spinodal decomposition, in: K. Gernot (Ed.), Phase Transformations in Materials, WILEY-VCH Verlag GmbH, Weinheim, 2001, p. 436.
[53] K. Binder, Nucleation barriers, spinodals, and the Ginzburg criterion, Phys. Rev. A: At. Mol. Opt. Phys. 29 (1984) 341.
[54] M.K. Miller, Atom Probe Tomography: Analysis at the Atomic Level, Kluwer Academic, Plenum Publishers, New York, 2000.
[55] M.K. Miller, Field evaporation and field ion microscopy study of the morphology of phases produced as a result of low temperature phase transformations in the iron–chromium system, J. Phys. Colloq. 50 (C8) (1989) 247–252.